Nwankwo *et al.*
Journal of Engineering and Applied Science (2022) 69:88
https://doi.org/10.1186/s44147-022-00139-8

Journal of Engineering and Applied Science

RESEARCH Open Access

Assessment of liquid and gas impingement cooling fluids with numerical solution for better steel austempering

Azubuike Michael Nwankwo[1*], Thomas Okechukwu Onah[2] and Bertrand Nduka Nwankwojike[3]

*Correspondence: zubbymike@gmail.com

[1] Department of Mechanical Caritas University Amorji-Nike Emene, Enugu, Nigeria
[2] Department of Mechanical and Production Engineering, Enugu State University of Science and Technology, Enugu, Nigeria
[3] Department of Mechanical Michael Okpara University of Agriculture Umudike, Umudike, Abia State, Nigeria

Abstract

Impingement jet heat transfer was studied using liquid and gas fluids to determine better cooling fluid. The materials used were rectangular steel plates of 230 mm by 120 mm by 12 mm, single jet diameters of 10–40 mm with impingement gaps of 115–155 mm. A computational fluid dynamics software application ANSYS 2020R1 was employed for simulation, and lumped thermal mass analysis was used for experimental modeling. The experimental results showed an increase in heat transfer coefficient with increased pipe diameters and with a corresponding increase in impingement gaps and flow rate. This revealed 265.4–383.9 W/m^2 K and 85.3–109 W/m^2 K at diameter 10 mm and 336.5–365 W/m^2 K and 109.0–137.5 W/m^2 K at diameter 40 mm for both water and air, respectively. Numerical simulation revealed heat flux of 22518–38.94 W/m^2 and 7570.2–4.25 W/m^2 and 6742.8–27.1 W/m^2 and 4155.6–6.1 W/m at diameters 10 mm and 40 mm, respectively. This confirmed that water remains a better cooling fluid with a 6.2% difference at the diameter of 10 mm and a 0.1% difference at the diameter of 40 mm. An acceptable error margin of 4 to 18% upon the comparison of empirical analysis with numerical simulation is obtained. The above suggests a better cooling rate for the microstructure of the steel using water against air.

Keywords: Single jet impingement, Lumped thermal mass, Liquid and gas, Numerical simulation, Impingement cooling fluid

Introduction

The jet impingement cooling process is a heat removal process that enables the removal of heat from a hot surface faster. Over the years, with the continual enhancement of steel material functions, the growing demand for cost cutting by reducing the use of alloying elements, and streamlining processes: the thermomechanical control process (TMCP), has become increasingly important [1, 2]. At one point of the designer's desired need, steel materials are subject to either of the following: bending and at the other to twisting, rotations, etc. Attending operations under these conditions requires certain specific properties to be able to successfully withstand the various conditions the designers subject them to [3]. Heat treatment, heating, and soaking at cooling temperature cycles steel are reduced, help before now to handle as much as possible, yet in recent times

could not do more [4, 5]. Opined that by restructuring its microstructure and physical structure with proper monitoring and controlling of its temperature during heating and cooling processes. Its usage with the evolving engineering and technology advancement is due to the designer's quest for newer applications, which causes the manipulation of steel's mechanical and metallurgical properties to the designer's desired design application. Therefore, there is a need for improving steel properties, which demand cost reduction in alloying elements, modeling, and streamlining processes, hence need for a better process [1]. In particular, the hot-rolling process, which is a well-known manufacturing method of steel strips, requires great management since it has a crucial influence on the properties of the final product [2].

Meanwhile, the modes of cooling by quenching process using different fluids opened it up for improvement. The era of controlled cooling opens up, an important part of thermomechanical controlled process (TMCP) technology, which significantly influences the microstructure and mechanical property of hot-rolled steel plates [6, 7]. As one of the important elements of this technology, the technique that allows the precise control of the fluid quenching temperature can be cited along with the metallurgical and controlled rolling techniques [1]. Therefore, jet impingement cooling, a type of accelerated controlled cooling, is a process used to achieve high heat removal yield from a heated material using the desired coolant for easy cooling. Steel production having desired mechanical and metallurgical properties requires accurate temperature control during the cooling process as noted by [8]. This work looks for a solution to the Leidenfrost phenomenon in water from another fluid.

Steel as an engineering material

Agreeing to the Society of Automobile Engineers and the American Institute of Steel, iron and steel are alloys of iron and carbon that normally have less than 1.0wt% of carbon [9]. It may contain other alloying elements at different compositions and/or heat treatment [10–12]. In this present work, we recognized three main grades of steel: low, medium, and high carbon steel with carbon content ranges of 0.015–0.30%wt for low carbon steel, 0.031–0.58%wt for medium carbon steel, and 0.6–2%wt for high carbon steel [13].

Hydrodynamics of jet impingement

Jet from the ROT cooling stage first exits the circular nozzle and impinges over the dry heated plate surface (free-surface jet), followed next by arrays that collide with the leftover fluid on the surface (plunging jet). These two types are mostly treated as free-surface jets in comparison with the submerged jet. Accordingly, [14] showed some types of single jet impingement cooling. This work uses a free-surface jet impingement cooling profile as shown in Fig. 1 below.

The flow of the liquid in impingement process can be divided arbitrarily into two zones, the impingement zone characterized by a sharp increase in the streamwise velocity and a parallel flow zone with a more gradual change of streamwise. Figure 1 depicts the streamwise velocity (u_i). In hydrodynamics, the streamwise at the stagnation point increase to the jet streamwise velocity V_{ji}. The hydrodynamics of circular jets differ from others in the parallel flow region. This is because the water velocity in the parallel flow

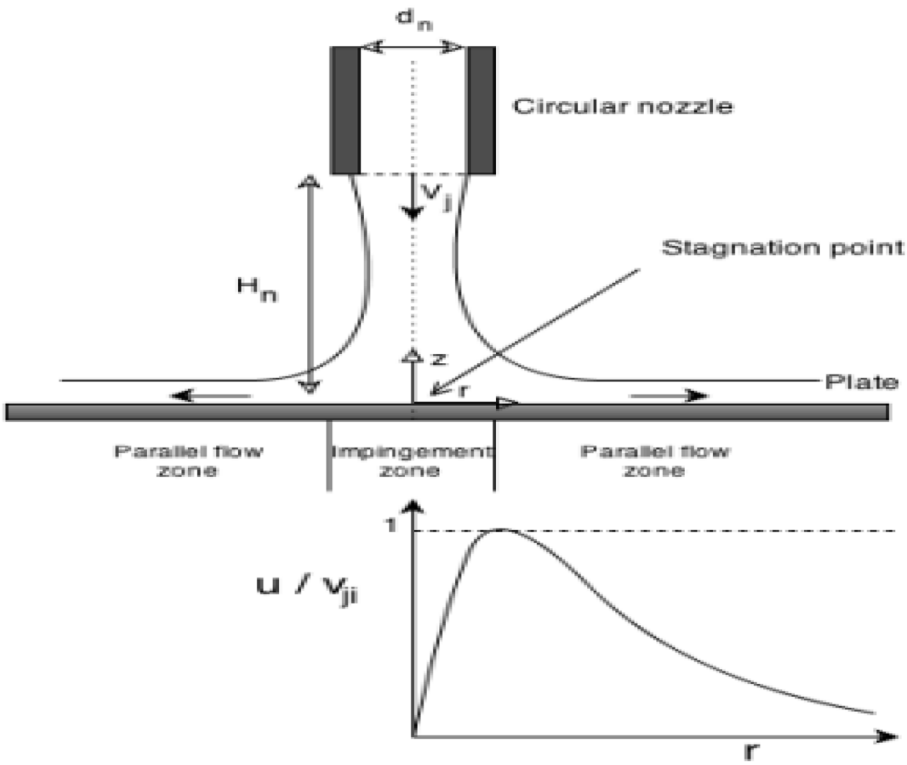

Fig. 1 Schematic of free-surface jet and liquid velocity profile parallel to surface circular jets [15]

zone of circular jets decreases, whereas the water velocity for the planar jet does not decrease [16].

Computational fluid dynamics

Numerical solution based on computational fluid dynamics (CFD) is the analysis of systems involving fluid flow, heat transfer, and associated phenomena such as chemical reactions using computer-based simulation; this technique is very powerful and spans a wide range of industrial and nonindustrial application areas [17]. CFD is an effective and powerful tool to numerically simulate fluid flow and heat transfer. The conventional methods which are the most popular in CFD are the finite element method (FEM), finite volume method (FVM), finite difference method (FDM), and spectral methods. These methods solve nonlinear Navier-Stokes equations which are governing equations for CFD describing popular conservation of mass, momentum, and energy equations [18]. The baseline results from CFD analysis are compared with experimental analysis, using ANSYS FLUENT and many other fluid flow software as studied by [2, 9, 19].

Many numerical models have been studied like SST k-w model while v^2f turbulence model for turbulence analysis because of its minimal error at the stagnation point and wall regions. Numerically, revealing that the ratio of the nozzle diameter to cylinder diameter affects Reynolds number value also showed that the RNG k-e model is better in predicting heat transfer characteristics. We found also that inlet turbulent intensity and eddy viscosity ratio are vital for the accurate prediction of realistic results using various RANS turbulence models; all these models are for fluid flow characteristics onto the hot

surface as studied by [20–23]. Nur et al. [24] studied hybrid nanofluid using single jet impingement cooling, and they showed that its heat transfer performance is highest and reduces the greatest amount of heat from the surface to the fluid. The models reviewed above are for the fluid and heated surface interaction. This work presents the knowledge in the behavior of the hot steel plate heat dissipation only. This has been uncertain in the literature for the single jet impingement cooling process. In the literature, it has been empirical analysis with minimal or no validation. Hence, this work assessed the behavior of controlled cooling of a hot-rolled steel plate using liquid and gas single jet impingement cooling by the transient thermal model of ANSYS fluent 2020R1.

Methods

The schematic of the modified run-out table system set-up plant is used and hoses the combined liquid and gas lines in the same headers. The location of these parts is shown on the schematic diagram in Fig. 2.

Experimental procedure

Based on impingement diameters, $D = 10$ mm and 40 mm with corresponding varying impingement gaps H, of 115 and 155 mm at two different controlled cooling temperatures of 150 °C and 110 °C, respectively. The experiments carried out were with a modified test rig, in Fig. 2. The assessment and numerical simulations were done using lumped thermal mass analysis, used to generate various values of heat transfer coefficient (h), and ANSYS was employed for simulation and 3-D modeling of the transient thermal model of the steel plate — 230 mm length by 120 mm width by 12 mm thickness, for temperature time and heat flux. The following test parameters based on Fig. 2 were used as experimental indicators: flow rate, nozzle velocity, constant impingement diameters, varying impingement gaps, surface temperatures, and controlled temperatures, cooling time, and rate.

The air jet impingement experiment was done using the same rig that has an air attachment nozzle at the flow valve close to the headers, with an air compressor

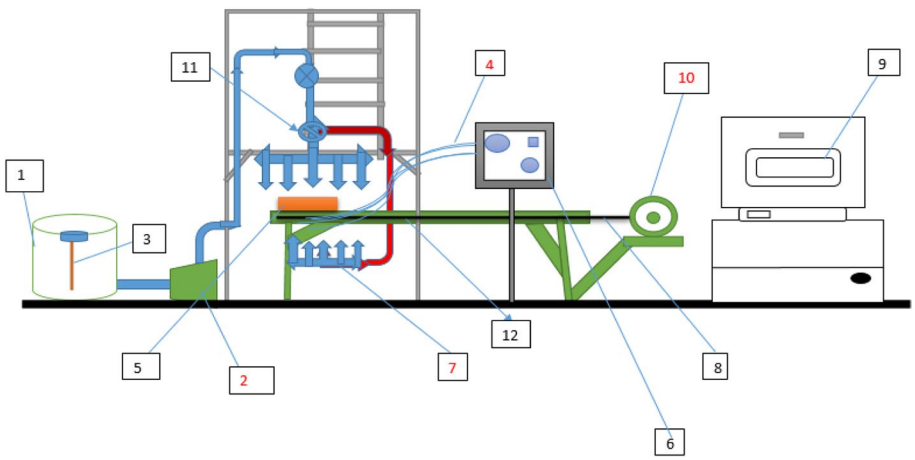

Fig. 2 Schematics of the modified ROT set-up plant: 1, water tank; 2, electric pump; 3, heater; 4, thermocouple wires; 5, the workpiece and its carrier; 6, thermocouple control panel, workpiece bed; 7, bottom impingement nozzle; 8, motorized screw conveyor; 9, furnace; 10, electric motor; 11, flow valve/air attachment nozzle; 12, flow meter; 13, ladder; 14, furnace support; 15, PVC pipes; 16, pressure gauge, 17

Table 1 Properties of sampled fluids

Properties of tiger nut						
S/N	**Fluids**	**Density (kg/m^3)**	**Viscosity (kg/M-S)**	**Thermal conduct W/MK**	**Specific heat J/KGK**	**Temp. °C**
1	W-JIC	1000	1.347×10^{-4}	0.609	500	50–60
2	A-JIC	1.164	1.849×10^{-5}	0.02551	1007	50–60

machine producing and supplying the air. Table 1 shows the properties of the sampled impingement fluids — liquid and gas (water and air).

Medium carbon steel plates with known varying chemical compositions and mechanical properties were obtained from the Ajaokuta Nigerian Steel Company with a steel grade of 0.56%C, the ultimate tensile strength of 957.1 Mpa, and Brinell hardness of 252.98 having an impact strength of 34.11 J.

Data analysis

This model of the impingement process is centered on the demonstration of transient-state heat conduction-convection across the sampled workpiece thickness of 12 mm, length of 230 mm, and width of 120 mm dimensions (Fig. 3).

$$MC\frac{d}{dt}(T_S - T_\infty) = -hA(T_S - T_\infty) \tag{1}$$

$$\frac{\partial(T_s - T_\infty)}{(T_s - T_\infty)} = \frac{-hAdt}{mcp} \tag{2}$$

Integration from $t = 0$ to $T = \mathrm{T_s}$:

$$\frac{T(t) - T_\infty}{T_i - T_\infty} = e^{-\alpha t} \tag{3}$$

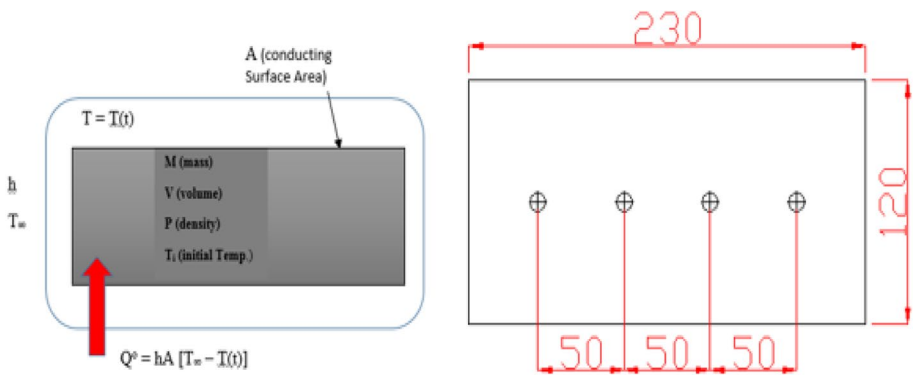

Fig. 3 Control volume of lumped thermal mass model analysis of impingement process

where α becomes the following:

$$\alpha \frac{hA}{mC_p} \tag{4}$$

The gradient is Eq. 4 given as in Eq. 5, as follows:

$$\text{The gradient is} - \propto = \frac{-hAt}{mcp} \tag{5}$$

$$\text{From which } h = \propto \rho wcp \tag{6}$$

where h is heat transfer coefficient W/m^2 k

$for\ steel, density\ \rho = \frac{7900hg}{m^3}$, $specific\ heat\ Cp = \frac{500J}{kgk}$, $sampled\ thickness\ w =$, $0.012m$

and $\propto$ is a gradient from Eq. (5)

Thereafter, a spread Excel sheet was used to estimate h Eq. (6), where $h = \propto \rho wc$, for $\propto$ being the slope based on lumped numerical experimental temperature-time plots. These values of convective heat transfer coefficient h were calculated.

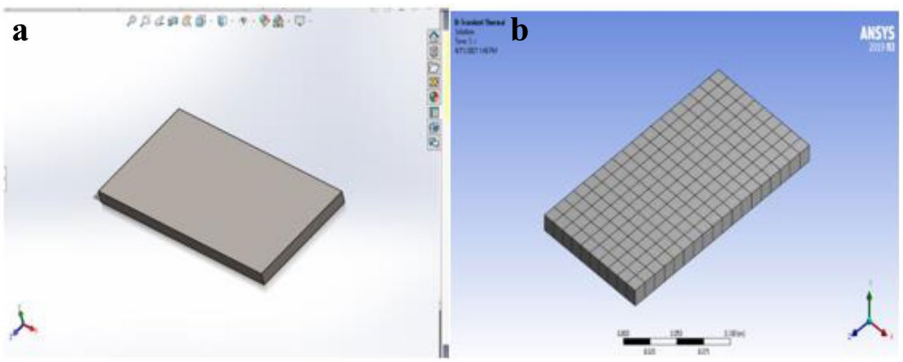

Fig. 4 **a** 3-d transient thermal model. **b** Mesh structure of the simulation

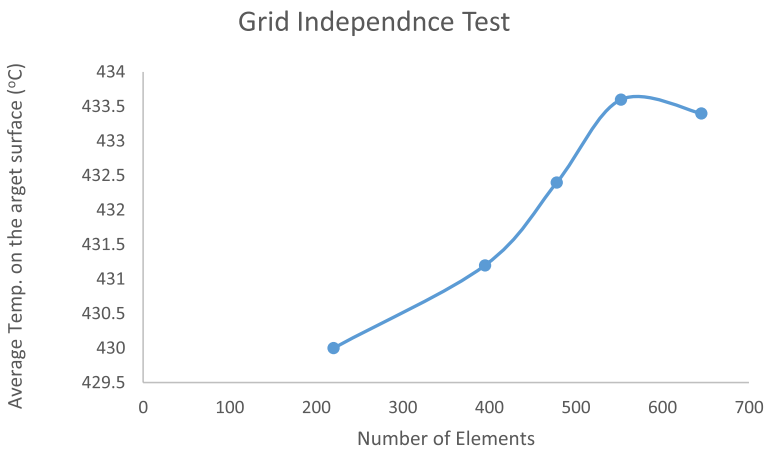

Fig. 5 Grid independence test

Table 2 150 °C at $D = 10$ mm variant T and H for W-JIC

$T = 450$ at $D = 10$ mm ($H = 115$)		$T = 440$ at $D = 10$ mm ($H = 125$)		$T = 430$ at $D = 10$ mm ($H = 135$)		$T = 420$ at $D = 10$ mm ($H = 145$)		$T = 410$ at $D = 10$ mm ($H = 155$)	
t(s)	Ts	t(s)	Ts	t(s)	Ts	t(s)	Ts	t(s)	Ts
0	450	0	440	0	430	0	420	0	410
40	400	35.5	391.7	32.4	383.3	29.3	375	25.5	366.7
80	350	71	343.4	64.8	336.6	58.6	330	51	323.4
120	300	106.5	295.1	97.2	289.9	87.9	285	76.5	280.1
160	250	142	246.8	129.6	243.2	117.2	240	102	236.8
200	200	177.5	198.5	162	196.5	146.5	195	127.5	193.5
240	150	213	150	194.4	150	175.8	150	153	150

Table 3 150 °C at D = 10 mm variant T and H for A-JIC

$T = 450$ at $D = 10$ mm ($H = 115$)		$T = 440$ at $D = 10$ mm ($H = 125$)		$T = 430$ at $D = 10$ mm ($H = 135$)		$T = 420$ at $D = 10$ mm ($H = 145$)		$T = 410$ at $D = 10$ mm ($H = 155$)	
t(s)	Ts	t(s)	Ts	t(s)	Ts	t(s)	Ts	t(s)	Ts
0	450	0	440	0	430	0	420	0	410
120.2	400	114.2	391.7	107.12	383.3	98.53	375	86.45	366.7
240.4	350	228.4	343.4	214.24	336.6	197.06	330	172.9	323.4
360.6	300	342.6	295.1	321.36	289.9	295.59	285	259.35	280.1
480.6	250	456.8	246.8	428.48	243.2	394.12	240	345.8	236.8
601.8	200	571	198.5	535.6	196.5	492.65	195	432.25	193.5
721.2	150	685.2	150	642.72	150	591.18	150	518.7	150

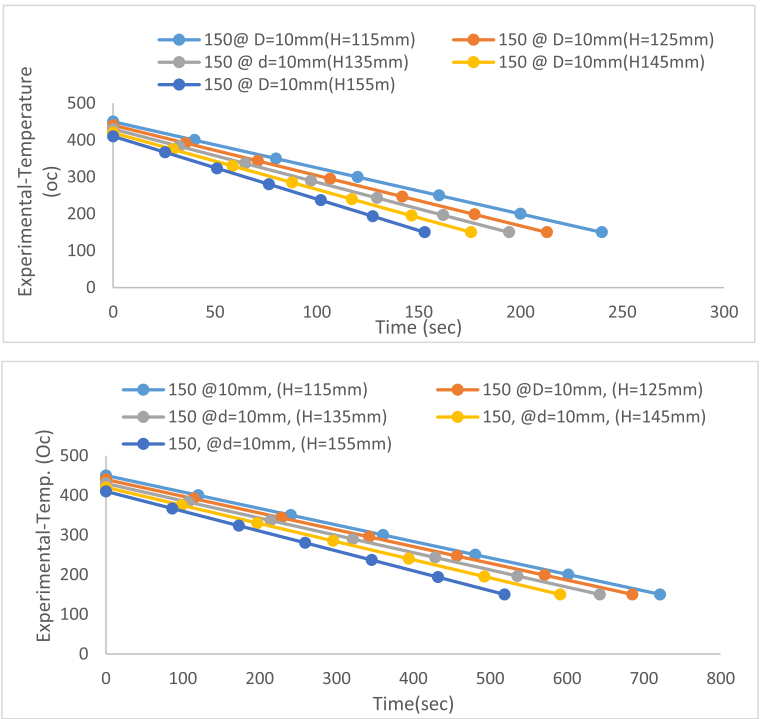

Fig. 6 Temperature time at 150 °C, $D = 10$ mm (top) for W-JIC and (bottom) for A-JIC

Table 4 110 °C at $D = 40$ mm variant T and H for W-JIC

***T* = 450 at D = 40 mm (*H* = 115)**		***T* = 440 at *D* = 40 mm (*H* = 125)**		***T* = 430 at *D* = 40 mm (*H* = 135)**		***T* = 420 at *D* = 40 mm (*H* = 145)**		**T = 410 at *D* = 40 mm (*H* = 155)**	
t(s)	***Ts***	**t(s)**	***Ts***	**t(s)**	***Ts***	**t(s)**	***Ts***	**t (s)**	**Ts**
0	450	0	440	0	430	0	420	0	410
44.6	393.34	42.6	385	41	376.67	40	368.34	39.2	360
89.2	336.68	85.2	330	82	323.34	80	316.68	78.4	310
133.8	280.02	127.8	275	123	270.01	120	265.02	117.6	260
178.4	223.36	170.4	220	164	216.68	160	213.36	156.8	210
223	166.7	213	165	205	163.35	200	161.7	196	160
267.6	110	255.6	110	246	110	240	110	235.2	110

Table 5 110 °C at $D = 40$ mm variant T and H for A-JIC

***T* = 450 at *D* = 40 mm (*H* = 115)**		***T* = 440 at *D* =4 0 mm (*H* = 125)**		***T* = 430 at *D* = 40 mm (*H* = 135)**		***T* = 420 at *D* = 40 mm (*H* = 145)**		***T* = 410 at *D* = 40 mm (*H* = 155)**	
t(s)	***Ts***	**t(s)**	***Ts***	**t(s)**	**Ts**	**t(s)**	***Ts***	**t(s)**	***Ts***
0	450	0	440	0	430	0	420	0	410
120.2	393.34	110.12	385	105.12	376.67	98.53	368.34	91.32	360
240.4	336.68	220.24	330	210.24	323.34	197.06	316.68	182.64	310
360.6	280.02	330.36	275	315.36	270.01	295.59	265.02	273.96	260
480.6	223.36	440.48	220	420.48	216.68	394.12	213.36	356.28	210
601.8	166.7	550.6	165	525.6	163.35	492.65	161.7	456.6	160
721.2	110	660.72	110	630.72	110	591.18	110	547.92	110

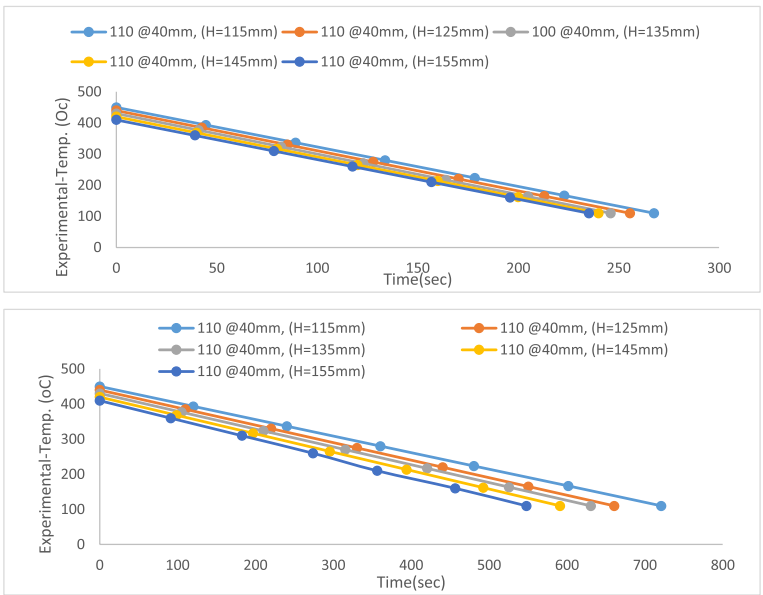

Fig. 7 Temperature time at 110 °C, $D = 40$ mm (top) for W-JIC and (bottom) for A-JIC

Table 6 Ln (theta) temperature time, $D = 10$ mm controlled at 115 °C W-JIC and A-JIC

Water impingement jet cooling (W-JIC)					Air impingement jet cooling (A-JIC)				
$T = 450$ °C at $D = 10$ mm ($H = 115$ mm)					$T = 450$ °C at $D = 10$ mm ($H = 115$ mm)				
T_s	T_f	Theta	t (s)	Ln (theta)	T_s	T_f	Theta	t (s)	Ln (theta)
450	50	1	0	0	450	45	1	0	0
400	50	0.875	40	−0.13353	400	45	0.876543	120.2	−0.13177
350	50	0.75	80	−0.28768	350	45	0.753086	240.4	−0.28358
300	50	0.625	120	−0.47	300	45	0.62963	360.6	−0.46262
250	50	0.5	160	−0.69315	250	45	0.506173	480.6	−0.68088
200	50	0.375	200	−0.98083	200	45	0.382716	601.8	−0.96046
150	50	0.25	240	−1.38629	150	45	0.259259	721.2	−1.34993

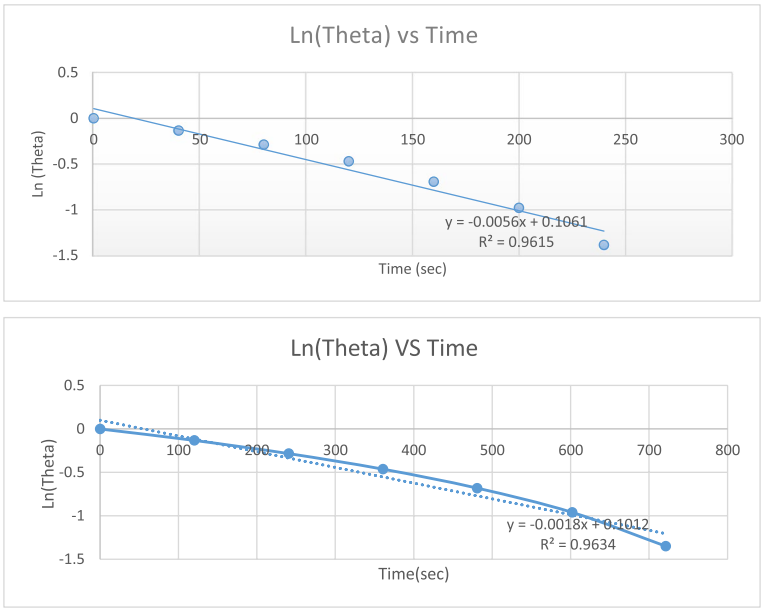

Fig. 8 Ln(theta) temperature time at 150 °C $D = 10$ mm (top) for W-JIC and (bottom) for A-JIC

Numerical simulation model

The simulation model is as shown in Fig. 4a which represents the hot steel plate 230 × 120 × 12 mm dimensions. The inlet nozzle diameters are 10 and 40 mm, while the impingement gaps are 115 and 155 mm. The mesh structure used in the study is in Fig. 4b. This study demonstrated a simple three-dimensional geometry simulation. The type of fluids used in the simulation is liquid and gas coolant with ANSYS transient thermal model for simulation.

Grid independence

To determine the ideal number of grids used and the impact of the number of elements on heat transfer and the final temperature of the target surface, the mesh was analyzed.

Table 7 Ln (theta) temperature time for $D = 40$ mm controlled at 110 °C A-JIC

Water impingement jet cooling					Air impingement jet cooling (A-JIC)				
$T = 450$ °C at $D = 40$ mm ($H = 115$ mm)					$T = 450$ °C at $D = 40$ mm ($H = 115$ mm)				
T_s	T_f	Theta	t(s)	Ln (theta)	T_s	T_f	Theta	t(s)	Ln (theta)
450	59	1	0	0	450	41	1	0	0
393.34	59	0.85509	44.6	−0.15655	393.34	41	0.861467	120.2	−0.14912
336.68	59	0.710179	89.2	−0.34224	336.68	41	0.722934	240.4	−0.32444
280.02	59	0.565269	133.8	−0.57045	280.02	41	0.584401	360.6	−0.53717
223.36	59	0.420358	178.4	−0.86665	223.36	41	0.445868	480.6	−0.80773
166.7	59	0.275448	223	−1.28936	166.7	41	0.307335	601.8	−1.17982
110	59	0.130435	267.6	−2.03688	110	41	0.168704	721.2	−1.77961

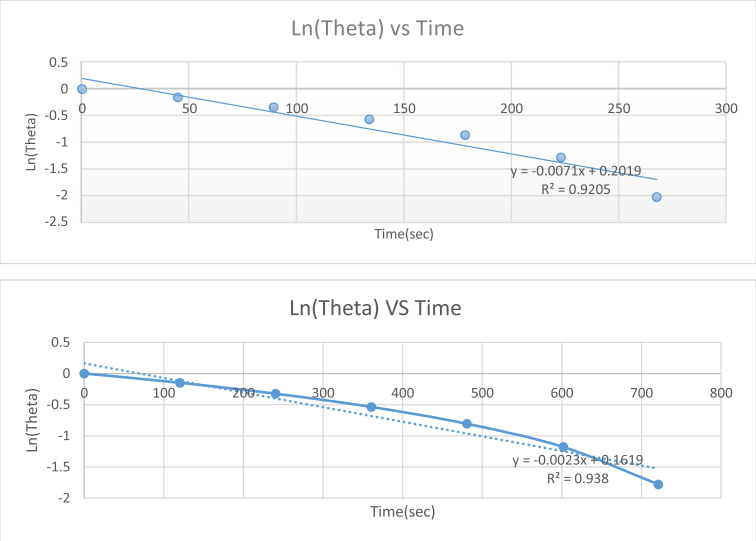

Fig. 9 Ln(theta) temperature time at 110 °C for $D = 40$ mm, (top) for W-JIC and (bottom) for A-JIC

Table 8 h for $D = 10$ and 40 mm at 150 °C and 110 °C for W-JIC and A-JIC

Fluids	D (mm)	H (mm)	Nozzle geo.	Vol. used qus. (m^3)	Time T (s)	Flow rate Q (m^3/s)/T (s)	T. water Tw (°C)	T. initial Ti (°C)	CHTC h (w/m^2 k)
W-JIC	10	115	11.5	0.39	240	0.001625	59	450	265.44
A-JIC	10	115	11.5	2.65	721.2	0.003674	41	450	85.32
W-JIC	40	155	15.5	0.09	235	0.000383	50	410	364.98
A-JIC	40	155	15.5	0.27	547.92	0.0004928	45	410	137.46

A coarse mesh with 552 number of elements and 0.02 m cell size employed in this study. Figure 5 shows the result of the grid independence test; additionally, patch conforming method and inflation method are applied to the geometry to ensure the flow of fluid near the target surface is well defined.

Boundary conditions

The boundary condition for the inlet velocity is determined based on the calculated Reynolds number. The inlet temperature and the surface temperature of the plate are set at 323 and in the range of 683 to 723 k for diameters of 10 mm and 40 mm, respectively. The temperature is set according to the working temperature of a microchip cooling system, which utilizes the fluid jet impingement cooling method of Nur et al. [24].

The final subcooled temperature was predetermined by the design in the range of 150 to 110 °C, and the heat transfer coefficient was calculated using LTMA and was inputted to ANSYS; thus, the wall heat flux was determined by the post-processing stage.

The Reynolds number used as the input parameter is in the range of 5000 to 250,000. The pressure treatment adopted the first-order upwind scheme for the turbulence numeric and the adventive scheme. While for the viscous model, a standard k-epsilon model was selected. The simulation was defined as converged at an RMS value lower than 1.0E−4. The results of the simulation are calculated throughout the computational domain during the simulation process.

Results and discussion

Experimental temperature-time evaluation

For controlled cooled temperature of 150 °C, diameter $D = 10$ mm. Results are presented in Tables 2 and 3, used for generating Fig. 6 and Tables 4 and 5 for Fig. 7 at D

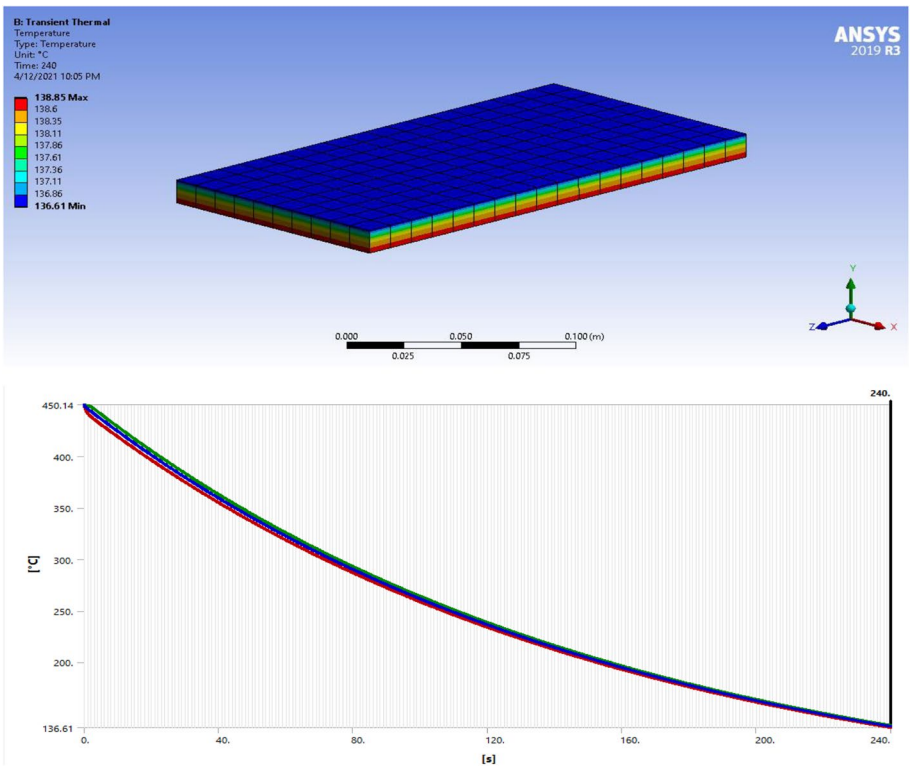

Fig. 10 CFD temp. time controlled model and plot at 150 °C, $D = 10$ mm, for W-JIC

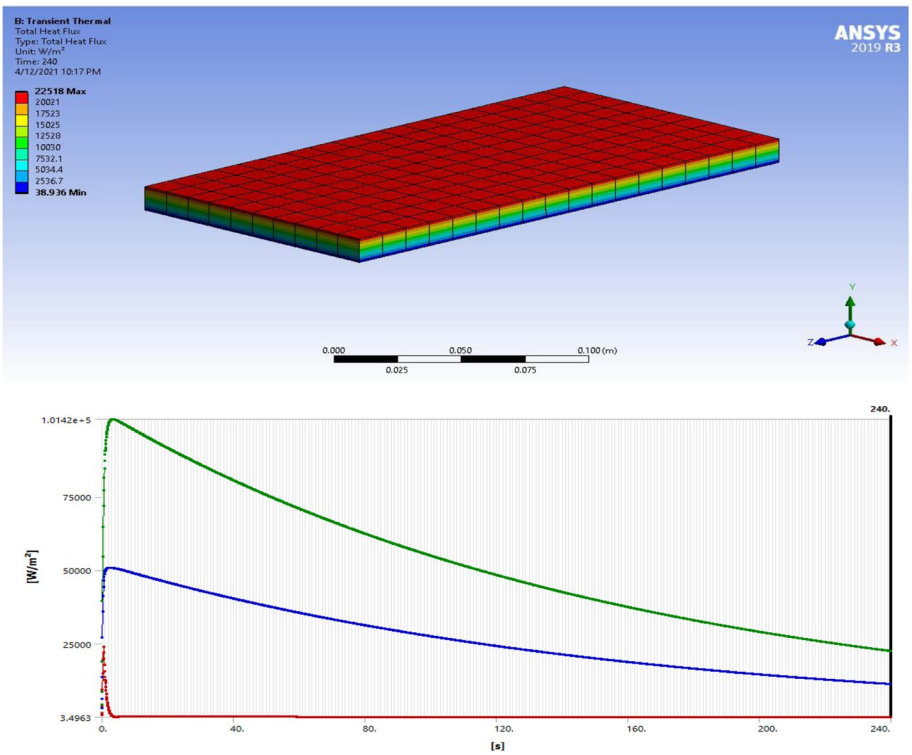

Fig. 11 CFD heat flux model and time plot at 150 °C, $D = 10$ mm, for W-JIC

$= 40$ mm and controlled cooling temperature of 110 °C that corresponds to W-JIC and A-JIC, respectively.

From all the graphs above, irrespective of the controlled cooled temperatures, the initial surface temperatures of hot-rolled steel plates showed the highest cooling time at a gap of 115 mm and lowest at a gap of 155 mm in each of the constant impingement diameters. This agrees with Onah, and Farial [25, 26] showing the same linear decrease.

Evaluated heat transfer coefficients (h) from LTMA

The results of the experiment for temperature time were then further analyzed by lumped thermal mass analysis which showed a linear decrease from various surface temperatures to various cooling times of the form $y = -\propto x + a$ for $R^2 = b$, where $\propto$ is the slope used for estimation of various convective heat transfer coefficient h from Eq. (5).

Ln (theta) for diameter $D = 10$ mm controlled at temperature of 150 °C is presented in Tables 6, for W-JIC and A-JIC used to generate Fig. 8, while Table 7 for W-JIC and A-JIC at diameter 40 mm is for Fig. 9 at different impingement gaps of 115 and 155 mm, respectively.

However, in all the controlled temperatures, the values of the slope of lumped thermal mass analysis$\propto$, in ln(theta) temperature against time for determining convective heat transfer coefficient (h), indicated a linear increase in impingement diameter D and a corresponding increase in impingement gap H. This is suggestive that the

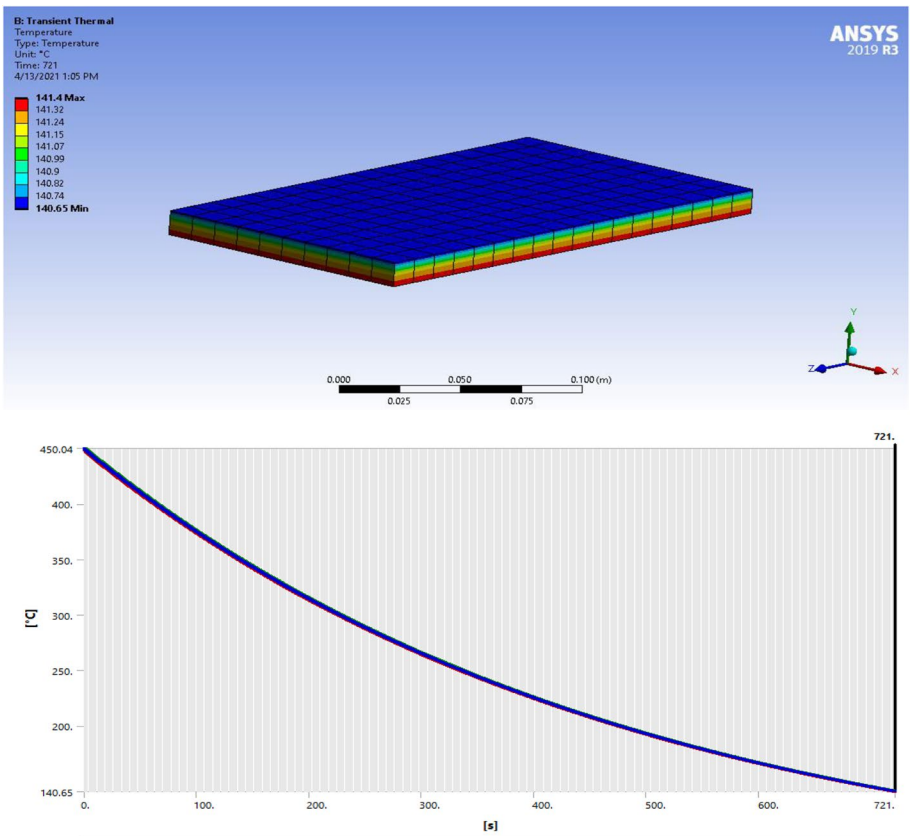

Fig. 12 CFD temp. controlled model and time plot at 150 °C, $D = 10$ mm, for A-JIC

various values of convective heat transfer coefficient (h) as obtained would be more at higher diameter D and higher impingement gap H, for proficient steel cooling, as studied by [27–29].

Heat transfer coefficient h from LTMA

Results of heat transfer coefficient (h) for $D = 10$ mm are presented in Table 8.

At constant diameter $D = 10$ mm, the convective heat transfer coefficient "h" showed an increase with increasing impingement gaps. Water has the highest values at both diameters and gaps. Flow rate decreased with increasing impingement gaps. The water decreased from 1.625×10^{-3} m^3/s to 4.9×10^{-4} m^3/s, and air decreased from 3.67×10^{-3} m^3/s to 4.43×10^{-4} m^3/s. This inferred that the lower the impingement gap H, the higher the flow rate Q.

For constant diameter $D = 40$ mm, convective heat transfer coefficient "h" maintained the same pattern, with water still having the highest.

This infers that at any given constant pipe diameter (D), flow rate (Q) decreases with a corresponding increase in impingement gap (H), resulting in increased convective heat transfer coefficient (h). This will give a proficient higher heat extraction rate on hot-rolled steel plates cooling in the steel mill industry and achieve designer desired micro-structures of steel, as also studied by [27–29].

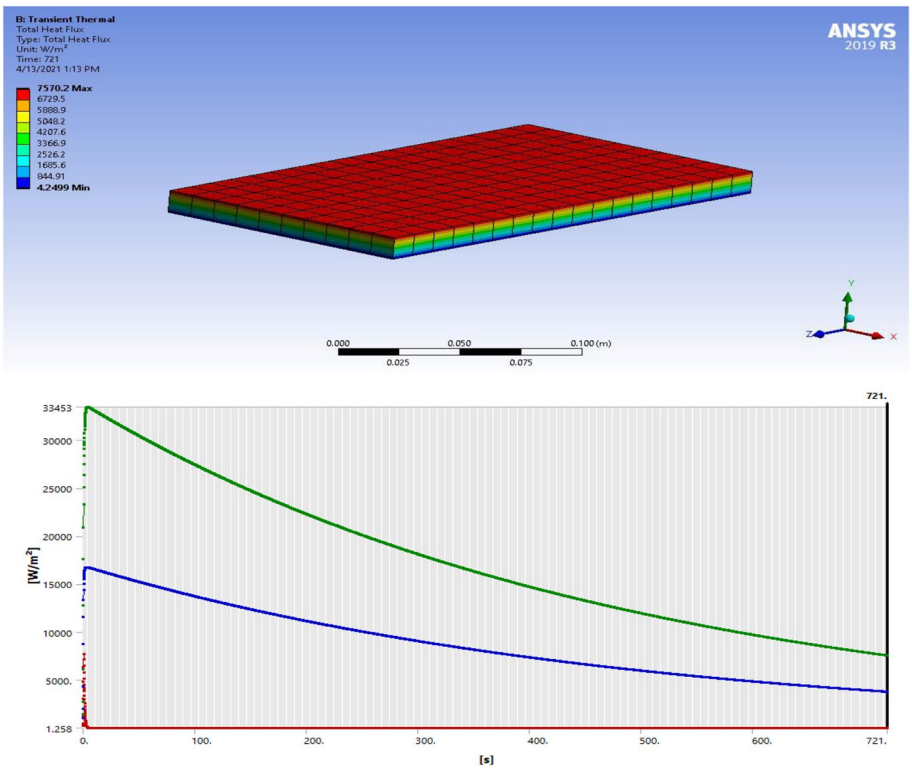

Fig. 13 CFD heat flux model and time plot at 150 °C, $D = 10$ mm, for A-JIC

Study of numerical simulation results

Figures 10 and 11 describe the CFD temperature-time controlled cooling model — region 1, is blue and totally cooled layer; region 2, is yellow, the middle layer, and partially cooled; and region 3, is red bottomed layer, gradually cooled, but still hotter than the two layers, Also, it indicates the temperature-time plot of the model, at each of the regions. The steeper curve region 1 showed where the convective heat transfer coefficient h was applied and slowly goes down to region 2 and to region 3, where heat flow was perfectly insulated that retained some hotness in the steel plate. Figures 12 and 13 represent the CFD-controlled heat flux model, where the top region showed the highest heat flux down to the bottom the lowest. Again, it also showed a plot of the heat flux against time. The rate of heat flux dissipation was 2.2×10^{-6} W/m^2/s and 1.74×10^{-7} W/m^2/s maximum for W-JIC and A-JIC, respectively.

Figures 14 and 15 describe the CFD temperature-time controlled cooling model, showing the same pattern as $D = 10$ mm, and CFD temperature-time plot, at each of the regions, having the same shape as the plot of $D = 10$ mm. Figures 16 and 17 represent the controlled heat flux model. It showed the same pattern of cooling as above, as well as showing a plot of the heat flux against time. The rate of heat flux dissipation was 1.10×10^{-7}W/m^2/s and 1.33×10^{-7}W/m^2/s maximum for W-JIC and A-JIC, respectively, which suggested water as a better impingement fluid as opined by [8, 26]. This dissipation of heat flux showed that water removes heat per unit area per second better than air in both diameters.

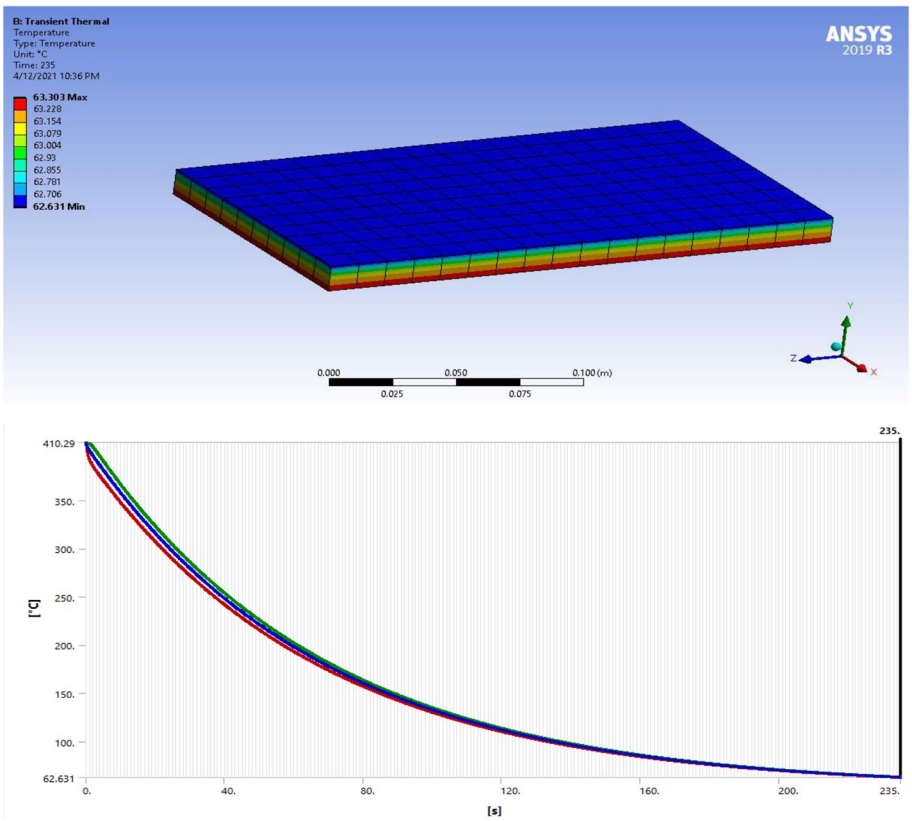

Fig. 14 CFD temp. controlled model and time plot at 110 °C, $D = 40$ mm, for W-JIC

Table 9 Heat fluxes at 150 °C for $D = 10$ mm and $D = 40$ mm for $H = 115$ mm

At $D = 10$ mm			At $D = 40$ mm		
Layers	**W-JIC (W/m^2)**	**A-JIC (W/m^2)**	**Layers**	**W-JIC (W/m^2)**	**A-JIC (W/m^2)**
Top	22518	7570.2	Top	6742.8	4155.6
Middle	12528	4207.6	Middle	3758.1	2311.4
Bottom	38.936	4.2499	Bottom	27.134	6.045

Table 10 Experimental and simulated data at 150 °C and 110 °C for $H = 115$ mm and 155 mm

At $D = 10$ mm				At $D = 40$ mm			
W-JIC		**A-JIC**		**W-JIC**		**A-JIC**	
t(s)	***Ts* °C**	**t(s)**	***Ts* °C**	**t(s)**	***Ts* °C**	**t(s)**	***Ts* °C**
0	450	0	450	0	410	0	410
40	400	120.2	400	39.2	360	91.32	360
80	350	240.2	350	78.4	310	182.64	310
120	300	360.6	300	117.6	260	273.96	260
160	250	480.6	250	156.8	210	356.28	210
200	200	601.8	200	196	160	456.6	160
240	150	721.2	150	235.2	110	547.92	110

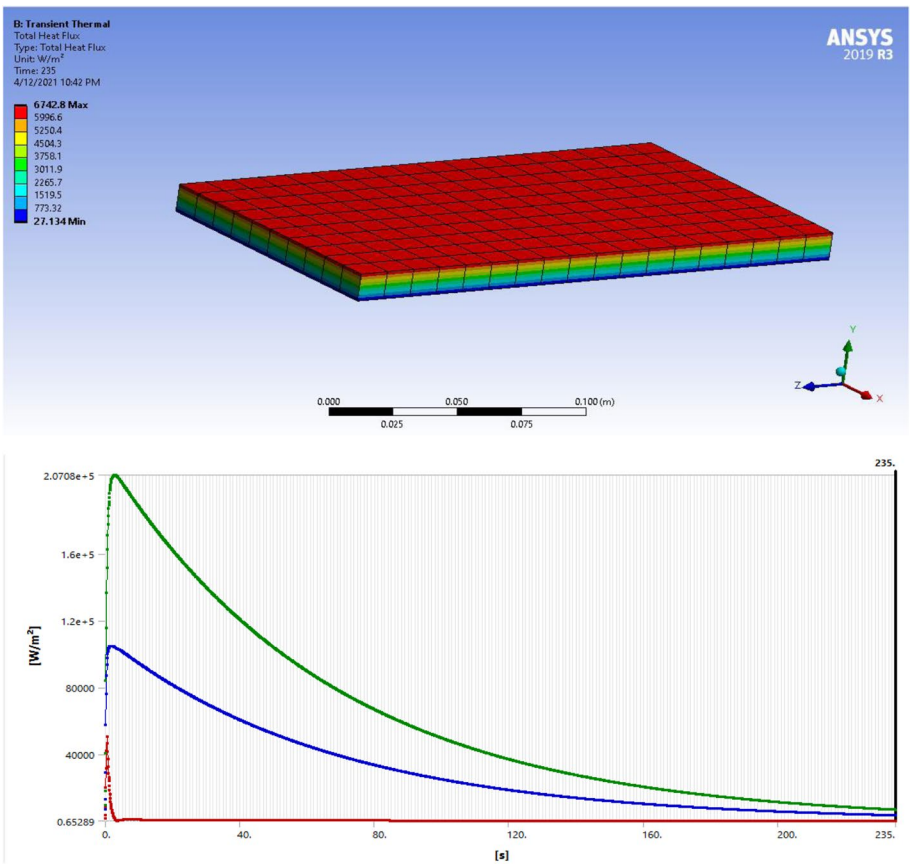

Fig. 15 CFD heat flux model and time plot at 110 °C, $D = 40$ mm, $H = 155$ mm for W-JIC

Table 11 Experimental uncertainties

Concomitant uncertainties	Parameters
Random uncertainty	1. Temperature uncertainty — randomly measuring the spread of temperature 2. Pressure uncertainty — randomly measuring the spread of pressure
Instrumental uncertainty	1. Flowmeter: instrumental uncertainty in measuring the rate of fluid flow of impingement fluid 2. Pressure gauge: this instrumental uncertainty is based on measuring the water pump pressure 3. Thermocouple: installation and testing instrumental uncertainty, based on the measuring hot rolled steel plate temperature 4. Volume flow rate measuring cylinder: instrumental uncertainty that happened as a result of measuring the used and unused water using a calibrated volumetric cylinder 5. Stopwatch: time uncertainty
Reduction uncertainty	1. Temperature reduction: the uncertainty is the percentage value of error and average temperature measured value 2. Pressure reduction: the percentage value of error and average pressure measured value

Table 9 showed the heat fluxes at $D = 10$ mm and 40 mm, highest at the top where the convective heat transfer coefficient value is more. Heat flux showed a 66.4% difference for $D = 10$ mm and 75.2 for $D = 40$ mm for W-JIC and A-JIC, respectively. Furthermore, heat fluxes decreased linearly from top to bottom, showing an increase in convective heat transfer coefficient with corresponding increasing impingement gap H.

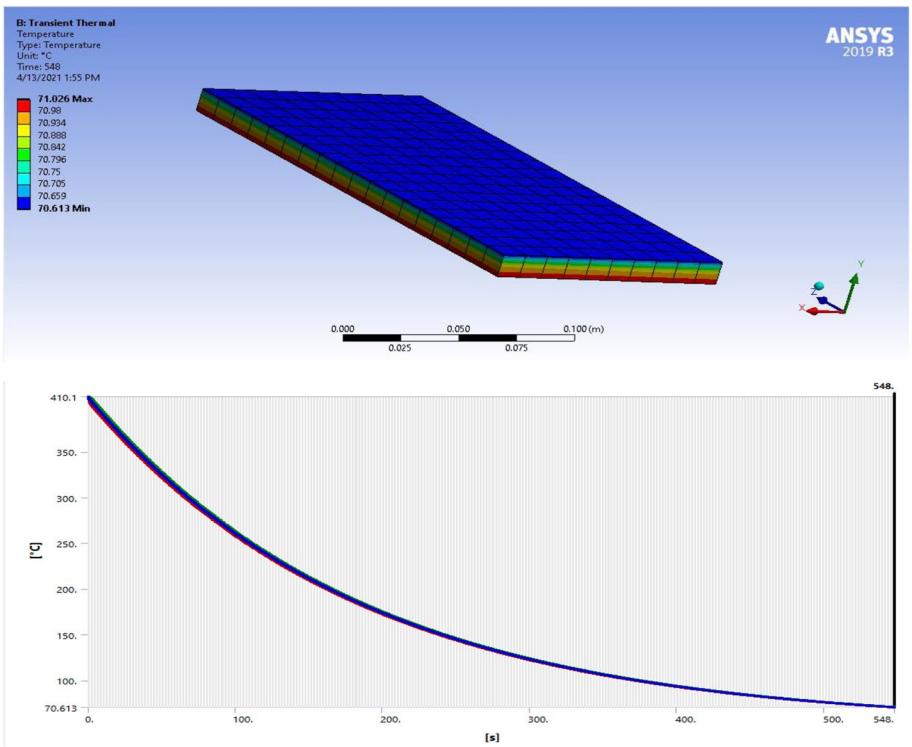

Fig. 16 CFD temp. controlled model and time plot at 110 °C, $D = 40$ mm, for A-JIC

Experimental and CFD numerical simulation temperature-time profile validation

Experimental and simulated data of both diameters are presented in Table 10 at convective heat transfer coefficient of h for water and h for air.

Table 10 showed the controlled temperature of 150 °C and 110 °C and initial temperature $T = 450$ °C and 410 °C for varied time t(s) for both experimental data and the ANSYS CFD simulation data plotted in Fig. 18 for both diameters. An acceptable error margin is of 4.5–6.6%. Confirming the affirmation, that water is a better fluid as specified by Md Lokman and Onah [25, 30].

Experimental uncertainties concomitant

The concomitant uncertainties in this work are the vital influences or limitations that are very expedient in the attainment of the set goal in this work, which is very grim to regulate. Thus, the plus or minus estimation uncertainties are ways of checkmating the errors in the measurement of these influences. These influences are underscored in Table 11.

Uncertainties for random measurement

Random uncertainties with absolute temperature values are as follows: for $D = 10$ mm, $H = 115$ mm at 150 °C, and for water $T = (450 + 440 + 430 + 420 + 410)/5 = 430$ °C. Meanwhile, the spread of temperature measurement ΔT is 0.9 °C; thus, $T = 430 \pm 0.9$ °C. Conversely, pressure random uncertainties were determined as follows: for $D = 10$ mm, $H = 115$ mm at 150 °C is ($2.5 \times 105 + 2.5 \times 105 + 2.5 \times 105 + 2.5 \times 105 + 2.5 \times$

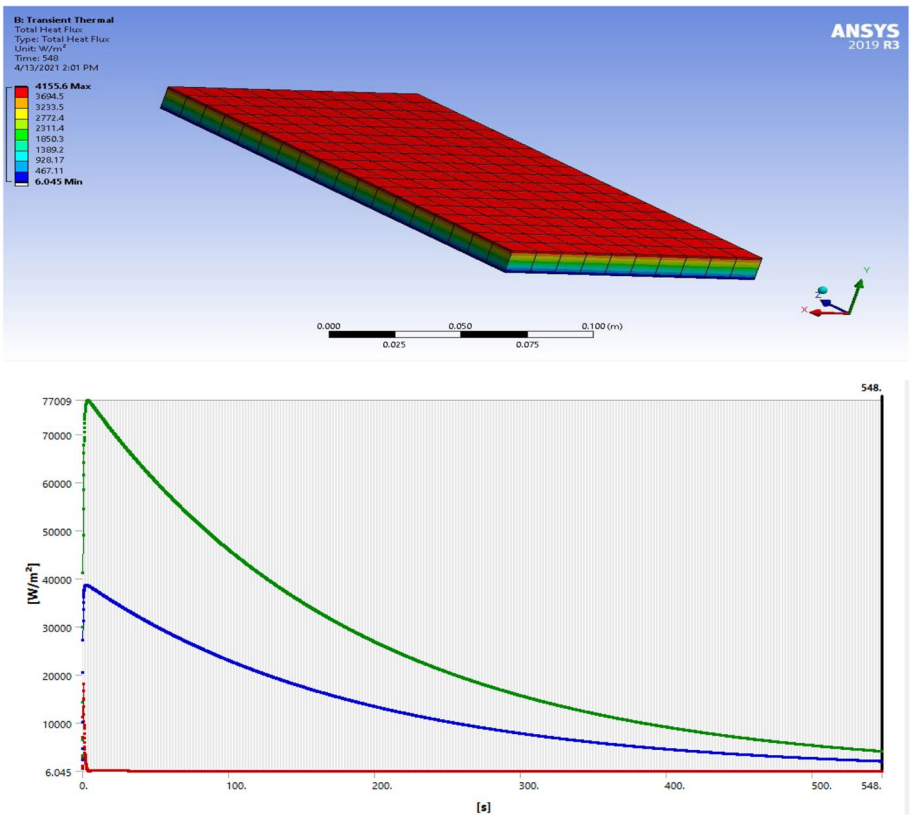

Fig. 17 CFD heat flux model and time plot at 110 °C, $D = 40$ mm, for A-JIC

105)/5 = 2.5 × 105 N/m^2, and equally the spread of pressure measurement ΔP is 0.1 × 105 N/m^2; thus, $P = 2.5 \times 105 \pm 0.1 \times 105$ N/m^2.

Uncertainties for random measurement

The water flow meter used has a specification of an accuracy: ± 1% of reading uncertainty tolerance; in addition, the water pump used has a current of 2.5 amp and a capacity of 0.5 hp. The pressure gauge calibrated was in the range of 0 to 10 bars with a measurement uncertainty tolerance of ± 0.1. In the testing and installation of the thermocouple, it recorded 97 °C with an error of ± 0.26 °C. The volumetric measuring cylinder calibrated was in the range of 50 to 500 mm^3 with ± 0.1 mm^3 uncertainty error. Similarly, the stopwatch calibrated was in the range of 0 to 60 s and at the top end with an accuracy uncertainty of ± 0.1.

Uncertainties for reduction measurement

For temperature, the uncertainty is for $D = 10$ mm, $H = 115$ mm at150 °C for water, and $T = 430$ °C, since the uncertainty in measure ΔT is 0.9 °C; thus, $T = 430 \pm 0.9$ °C, and then, reduction temperature uncertainty is (0.9/430) × 100 = 21%. In the pressure reduction uncertainty, $D = 10$ mm, $H = 115$ mm at150 °C, and $P = (2.5 \times 105$ N/m^2). The associated uncertainty measurement ΔP is 0.1 × 105 N/m^2; thus, $P = (2.5 \times 105 \pm$

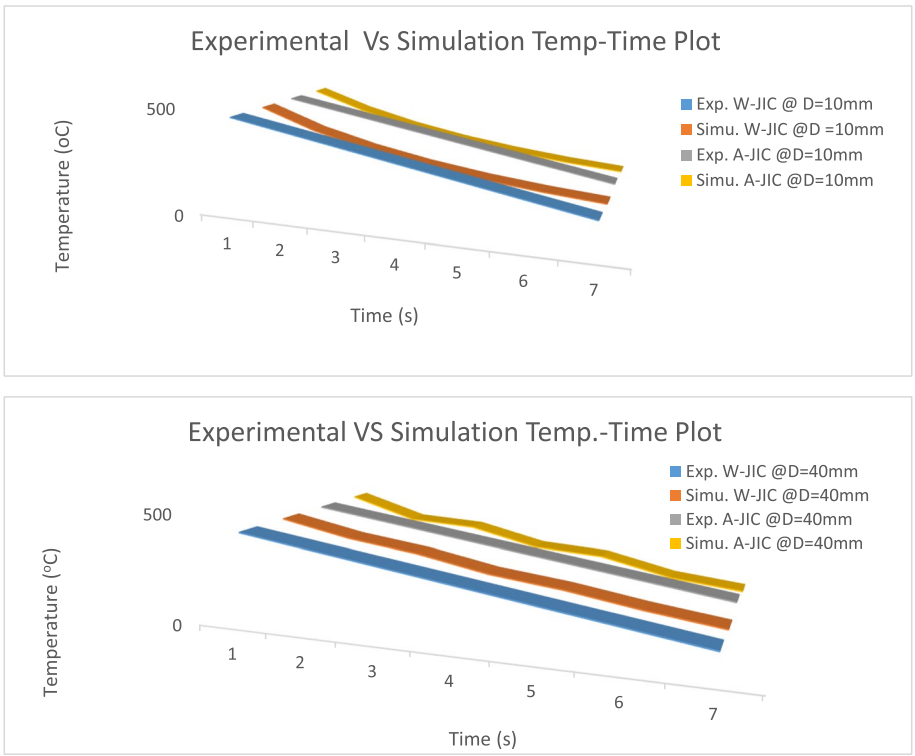

Fig. 18 Experimental and simulation temp-time plot, top for $D = 10$ mm and (bottom) for $D = 40$ mm

0.1×105 N/m^2), and then, reduction pressure uncertainty is $(0.1 \times 105/2.5 \times 105) \times 100 = 40\%$.

Conclusions

This study involved a comparative study of jet impingement fluids. Empirical results using lumped thermal mass analysis revealed convective heat transfer of 265–365 W/m^2 K and 85–138 W/m^2 K for W-JIC and A-JIC, respectively at diameters of 10 mm and 40 mm. CFD numerical simulation revealed maximum heat fluxes of 22518 W/m^2 and 6742.8 W/m^2 for water and 7570.2 W/m^2 and 4155.6 W/m^2 for air at 10 mm and 40 mm, respectively. This confirmed water as the best impingement cooling fluid with a 6.2% difference at a diameter of 10 mm and a 0.1% difference at a diameter of 40 mm. validation of empirical results with numerical simulation results showed an acceptable error margin of 4 to 18% for diameters 10 mm and 40 mm, respectively. Certainly, with Kandilkar [31] study, this further confirms results in the literature that water will give a proficient higher heat extraction rate on hot-rolled steel plates in the steel mill industry.

Abbreviations

A-JIC	Air jet impingement cooling
ANSYS	Analytical system
A	Area (m^2)
CFD	Computational fluid dynamics
Cp	Specific heat capacity (J/kg k)
D	Diameter (mm)
ESUT	Enugu State University of Science and Technology
h	Heat transfer coefficient (w/m^2 k)

H	Impingement gap (mm)
FEM	Finite element method
FVM	Finite volume method
FDM	Finite difference method
LTMA	Lumped thermal mass analysis
M	Mass (kg)
MME	Metallurgical and material engineering
PVC	Polyvinyl chloride
P	Pressure (N/m^2)
Q	Flow rate (m^3/s)
ROT	Run-out table
RMS	Root mean square
T	Initial temperature (°C)
T_{sub}	Subcooled temperature (°C)
T∞	Infinite temperature (°C)
TMCP	Thermomechanical cooling process
t	Time (s)
u_i	Streamwise velocity (m/s)
v_{ij}	Streamwise jet velocity (m/s)
W-JIC	Water jet impingement cooling
w	Thickness (m)
ΔT	Change in temperature (°C)
ΔP	Change in pressure (N/m^2)
P	Density (kg/m^3)

Supplementary Information

The online version contains supplementary material available at https://doi.org/10.1186/s44147-022-00139-8.

Additional file 1.

Acknowledgments
Not applicable.

Authors' contributions
AN wrote up the manuscript. TO and AN conducted the laboratory experiments. BN supervised the laboratory experiment and structured, edited, read, and approved the final manuscript. The authors read and approved the final manuscript.

Authors' information
AN is currently a lecturer, at the Department of Mechanical Engineering Caritas, Enugu. TO is a lecturer, Department of Mechanical and Production Engineering, Enugu State University of Science and Technology, Enugu state. BN is currently a Professor of Mechanical Engineering, at Michael Okpara University of Agriculture Umudike, Abia state.

Funding
No funding was obtained for this study.

Availability of data and materials
The datasets supporting the conclusions of this article are included in the article.

Declarations

Competing interests
The authors declare that they have no competing interests.

Received: 1 June 2022 Accepted: 28 August 2022
Published online: 01 October 2022

References

1. Kazuaki K, Osamu N, Yoichi H (2016) Water Quenching CFD (Computational Fluid Dynamics) Simulation with Cylinderical Impinging Jets. In: NIPPON Stell and SUMITOMO Metal Technical Report. Tiabah University of Saudi Arabia, Scholl of Post Graduate studies, Osaka
2. Alqash SI (2015) Numerical Simulations of Hydrodynamics of multiple water jet impinging over a horizontal moving plate. In: Numerical Simulations of Hydrodynamics of multiple water jet impinging over a horizontal moving plate. University of British Columbia, Vancouver; p 125.
3. Anthonio AG, da Silveira JHD (2014) Accelerated Cooling of Steel Plates: The Time has Come. J ASTM Int 5:8–15
4. Purna (2013) Model Based Numerical State Feedback Control of Jet Impingement Cooling of a Steel Plate by Pole Placement Technique. Int J Comput Eng Res 03(8):2205–3005

5. Yongjun Z (2015) The Cooling of a Hot Steel Plate by Impinging Water Jet. Wollongong university, Australia
6. Xie Q (2016) Heat Transfer Coefficient and Flow Charateristic of hot Steel Plates Cooling by Multiple Inclined Impinged Jets. ISIJ Int 5(8):1-7
7. Ade (2011) Effect of Heat Treatment on the Mechanical Engineering Essay. In: 1st International Conference on Experiments/process/system Modelling/Simulation/Optimization Intelligence. Tiabah University of Saudi Arabia, Scholl of Post Graduate studies, London
8. Molana (2013) Investigation of Heat Processes Onvolved in Liquid Impingement Jets: A Review. Braz J Chem Eng 03(30):413–435
9. Webb, Ma (2015) Single-Phase Liquid Jet Impingement Heat Transfer. J Acad Press Impingement Heat Transfer 26(126):105–115
10. Moukalled F, Managani LA (2016) Finite Volume Method in Computational Fluid Dynamics, Advanced Introduction with OpenFOAM and Matlab. Springer International, Switzerland
11. Ujam AJ, Onah T, Chime TO (2012) Effect of heat flow rate Q on convective heat transfer H, of fluid jet impingement cooling on hot plate. Int J Industr Eng A Technol 2(2):16–30
12. Ujam AJ, Onah T (2013) Effect of Jet Reynold's Number on Nusselt Number for Convective Impingement Air Cooling on a Hot Plate. J Energy Technol Policy 3:10
13. Ujam A, Ojobor SN, Onah TO (2012) Effect of coolant mass flow rate G on coefficient of convective heat transfer, H on a hot plate. WEEJS Int J Arts Combined Sci 3:1
14. Incorpera (2015) Advances in Heat Transfer. Academic press, Massachusetts
15. Rahman SM, Simanto MdH (2016) Effect of heat treatment on low carbon steel: An experimental Investigation; International Conference on materials and amnufacturing Engineering, Applied mechanics and materials 860(7). https://doi.org/10.4028/www.scientific.net/AMM.860.7.
16. M. John (2011) https://www.efunda.com/materilas/material_home/materilas.cfm
17. Jeffery A (2011) Advanced Engineering Mathematics. Academic press, Massachusetts
18. Verteeg et al (2017) An Introduction to Computational Fluid Dynamics: The Finite Element Method. Pearson Education Publishing, Edinburgh
19. Autulkumar K, Singh D (2019) Comparison of Various RANS models for impinging Round Jet Cooling from a cylinder. ASME J Heat Transfer 141(6):064503
20. Khurmi, Sedha (2012) Theory of Metal on Carbon Steels and Mechanical Properties of Medium Carbon Steel
21. Gilles GG, Vladan PA (2019) Modeling of Transient Bottom Jet Impingement Boiling. Elesevier Int J Heat Mass Transfer 136:1160–1170. https://doi.org/10.1016/j.ijheatmasstransfer.2019.03.060.
22. Onah TO, Ekwueme BN, Odukwe A, Nduka NB, Orga AC, Egwuagu MO, Chukwujindu S, Diyoke C, Nwankwo AM, Asogwa CT, Aka CC, Enebeh K, Asadu C (2022) Improved design and comparative evaluation of controlled water jet impingement cooling system for hot roll steel plates. Elseiver Int J Thermofluids 15:100172
23. Md Lokman, H. A., "Literature Review of Accelerated CFD Simulation Methods towards Online Application," The 7th International Conference on Applied Energy , Elsevier Energy Procedia, 75, pp. 3307-3314, 2015.
24. Dushyant S, Premachandran B, Sangeeta K (2013) Numerical Simulation of the Jet Impingement Cooling of a Circular Cylinder. Taylor and Francis Numerical Heat Transfer J Comput Method 64:2
25. Joseph I, Dushyant S, Saurabh K (2019) Experimental and Numerical Investigation of Heat Transfer Charateristics of Jet Impingement on a Flat Plate. Springer J Heat Mass Transfer 56:531–546
26. Kandlikar SABA (2007) Evaluation of Jet Impingement Spray and Microchannel Chip Cooling Options for High Heat Flux Removal. Heat Transfer Eng 28(11):911–923
27. Nur SM, Hanaf WA, Ghopa W, Zulkifli R, Abdullah S, Harun Z, Mansor MRA (2022) Numerical simulation on the effectiveness of hybrid nanofluid in jet. In: TMREES22-Fr, EURACA, 09 to 11 May 2022, Metz-Grand Est, France. Metz-Grand Est
28. Cemil Y, Nedim S, Yao SC, Hasan Riza GA (2011) Experimental Measurement and Computational Modeling for the Spray Cooling of a Steel Plate Near the Leidenfrost Temperature. J Thermal Sci Technol 31:27–36
29. Pallavi CC, Ashish NS (2017) Experimental and CFD Analysis of Jet Impingement Cooling on Copper Circular Plate. World J Eng Res Technol III(5):256–267
30. Callister, Phase Transformation of Microstrutural Formation from Austenite, 2012.
31. Farial (2012) Flow Visualization and heat transfer characteristic of liquid jet impingement. Int J Comput Method Eng Mech 13(4):239–253

Publisher's Note